



HAL
open science

Influence of electrolyte ageing on the Plasma Electrolytic Oxidation of aluminium

J. Martin, P. Leone, A. Nominé, D. Veys-Renaux, G. Henrion, T. Belmonte

► **To cite this version:**

J. Martin, P. Leone, A. Nominé, D. Veys-Renaux, G. Henrion, et al.. Influence of electrolyte ageing on the Plasma Electrolytic Oxidation of aluminium. *Surface and Coatings Technology*, 2015, 269, pp.36-46. 10.1016/j.surfcoat.2014.11.001 . hal-03612241

HAL Id: hal-03612241

<https://hal.univ-lorraine.fr/hal-03612241>

Submitted on 25 Jan 2023

HAL is a multi-disciplinary open access archive for the deposit and dissemination of scientific research documents, whether they are published or not. The documents may come from teaching and research institutions in France or abroad, or from public or private research centers.

L'archive ouverte pluridisciplinaire **HAL**, est destinée au dépôt et à la diffusion de documents scientifiques de niveau recherche, publiés ou non, émanant des établissements d'enseignement et de recherche français ou étrangers, des laboratoires publics ou privés.



Distributed under a Creative Commons Attribution - NonCommercial - NoDerivatives 4.0
International License

Influence of electrolyte ageing on the Plasma Electrolytic Oxidation of aluminium

J. Martin^{1,2*}, P. Leone¹, A. Nominé¹, D. Veys-Renaux¹, G. Henrion^{1,2}, T. Belmonte¹

¹ Université de Lorraine, UMR CNRS 7198, Institut Jean Lamour – Département Chimie et Physique des Solides et des Surfaces, Parc de Saurupt – CS 50840, F-54011 Nancy cedex France

² Université de Lorraine, Laboratoire d'Excellence Design of Alloy Metals for low-mAss Structures ('LabEx DAMAS'), Ile du Saulcy, F-57045 Metz cedex France

*Corresponding author: Tel.: +33 383 584 251

julien.martin@univ-lorraine.fr,

Abstract

The chemical stability of the electrolyte in Plasma Electrolytic Oxidation (PEO) has been the subject of much systematic investigation. The present study reports on experimental results on the ageing of a usual PEO electrolyte and its effect on the oxidation of the Al2214 aluminium alloy. A solution of potassium hydroxide ($[\text{KOH}] = 1 \text{ g.L}^{-1}$) and sodium silicate ($[\text{Na}_2\text{SiO}_3] = 1.65 \text{ g.L}^{-1}$) diluted in deionized water was either aged by running a process during 8 h at most or not. Comparison between materials treated in either solution was made next. Cross-checked experimental results from analytical chemistry, plasma diagnostics and materials science clearly evidence the effect of ageing of the electrolyte on the PEO process behaviour. The transition from arc to "soft" regime occurs earlier (from 18 min to 13 min processing time) as the electrolyte gets older. The concomitant decrease in the electrolyte electrical conductivity (from 7.5 mS.cm^{-1} to 6.8 mS.cm^{-1}) is correlated with changes in the ionic species

content in the electrolyte. Fast video-imaging (125 kfr./s) reveals that the micro-discharge characteristics are also sensitive since they become less numerous per area and unit time (from $220 \times 10^3 \text{ cm}^{-2} \text{ s}^{-1}$ to $120 \times 10^3 \text{ cm}^{-2} \text{ s}^{-1}$), exhibit shorter lifetime and have smaller sizes as the electrolyte ages. SEM observations of the as-grown coatings combined with roughness measures indicate a decrease in coating thickness ($\sim 20\%$) and roughness ($\sim 30\%$) while species from the electrolyte accumulate in the outer porous layer simultaneously with a gradual enrichment in $\alpha\text{-Al}_2\text{O}_3$ phase in the inner compact layer (from 36% to 43%). Finally, within the PEO conditions that were used, it is shown that the ageing phenomenon of the PEO electrolyte starts to influence the process after 2 hours aged.

Keywords : plasma electrolytic oxidation (PEO), aluminium, electrolyte ageing, oxide coating, micro-discharges, fast-video imaging.

1 Introduction

Plasma electrolytic oxidation (PEO) is a surface engineering process suitable for light weight metals (Al, Mg, Ti) and their alloys to form protective ceramic coatings [1]. Based on an electrochemical conversion of the metal surface, the rapid growth of the oxide layer takes place at potentials above the dielectric breakdown voltage of the insulating layer, leading thus to the development of numerous short-lived micro-discharges over the processed surface [2-4]. The resulting PEO coating exhibits improved surface performances in terms of adhesion, hardness, wear protection and corrosion resistance. As it uses diluted alkaline electrolytes, the PEO process complies with the present environmental and health regulations. Therefore it gains a growing interest in various industrial domains (transport, energy, medicine) to replace conventional chromic or sulphuric acid anodizing processes.

Researches devoted to improve the efficiency of the PEO process are abundant in the literature and one particular way consists in adjusting the right chemical composition of the electrolyte [1]. Electrical conductivity and basicity of the PEO electrolytes are commonly adjusted by addition of alkaline reagents as potassium hydroxide (KOH) or sodium hydroxide (NaOH) which provide both enhanced growth rate and improved tribological behaviour of the oxide-like ceramic coatings (Al_2O_3 , MgO, TiO_2) [5]. Furthermore, additives such as silicate (Na_2SiO_3) and aluminate (NaAlO_2) are widely used in order to reinforce the corrosion resistance and thermal barrier properties of Al and Mg oxides and their compounds [6-9]. The formation of stable products such as Mg_2SO_4 , MgAlO_4 , $3(\text{AlO}_3).2(\text{SiO}_2)$ that act as barrier layers prevents corrosion of alloys in the most corrosive environments. In recent years, thorough investigations have demonstrated the positive influence of new electrolyte additives (phosphate, fluoride, borate) on the performance of PEO films formed on magnesium and aluminium alloys [10-14]. Some authors have proposed to incorporate suspended nano-

particles (Al_2O_3 , ZrO_2 , TiO_2 , TiC) in the electrolyte to reduce the porosity of the PEO oxide layer and to improve the wear resistance of the formed coatings [15-18].

Few works deal with the chemical stability of the PEO electrolytes with the effective ageing time over successive treatments. Ageing phenomena, which could affect the final layer characteristics, are usually neglected. From an industrial point of view, the issue of the chemical stability of the electrolyte is of crucial importance in order to guarantee the highest reproducibility of the sought-after properties with the minimum process intervention. Regarding conventional anodizing processes such as chromic acid anodizing (CAA) or sulfuric acid anodizing (SAA), ageing of the treatment baths (cleaning, sealing, painting) is controlled empirically by manufacturers who limit the drifts in chemical composition by continuously renewing and tuning the content of chemical reagents. In a recent paper Terleeva *et al.* [19] evidenced the variations in the elemental composition of a silicate – alkaline electrolyte characteristics with ageing time (mainly a decrease in concentration of OH^- and Si^{4+} and increase in Al^{3+}), expressed in terms of accumulated charge quantity flowing through the investigated electrolyte. Their findings revealed that such variations in the electrolyte have a substantial influence on the PEO coating characteristics such as a decrease in the coating thickness and a substantial increase in the degree of aggregation of electrolyte components (Si, Na, K) at the top most surface of the oxide layer.

However, researches on the ageing of the PEO electrolyte are scarce. In this context, the aims of the present study are mainly to confirm such previous results and to correlate variations of both the electrolyte state and the PEO layer characteristics with the micro-discharge behaviour as the electrolyte gets aged. For this purpose, an experimental investigation of the electrolyte ageing during the PEO treatment of an aluminium alloy is reported. The selected electrolyte consists in a standard PEO electrolyte containing sodium silicate Na_2SiO_3 and potassium hydroxide KOH diluted in deionized water. The ageing process in the electrolyte

has been evidenced by taking into account several criteria based on the process monitoring data (voltage- and current-time responses), the electrolyte chemistry (conductivity and ionic species content), the micro-discharges behaviour (density, spatial distribution, size and lifetime) and the material characterization (layer morphology, roughness, thickness, element composition and alumina phase content). Finally, we shall discuss on correlation between the formation process of the oxide ceramic layer and the characteristics of the micro-discharges appearing at the surface of the processed sample in relation with the ageing process in the PEO electrolyte.

2 Experimental procedure

The experimental set-up consists basically of a 25 L electrolysis tank filled with the electrolyte. Rectangular samples of dimensions 50 mm × 30 mm × 6 mm (see Fig. 1) made of commercial 2214 grade aluminium alloy were used as substrate in this study (content in weight %, 3.9 – 5 Cu, 0.5 – 1.2 Mg, 0.4 – 1.2 Mn, 0.5 – 1.2 Si, 0.5 Fe, 0.5 Ti, 0.25 Zn, Al as balance). Prior to process, all the samples were ground down to 1200 SiC paper, ultrasonically degreased in acetone, dried in warm air, and then immersed in the electrolyte tank. The sample (anode) is located between two titanium counter-electrode plates (cathodes), of size 200 mm × 200 mm × 1 mm. The gap between each counter-electrode and the sample is set at 55 mm. Therefore, the active electrode area to electrolyte volume ratio is about $1.6 \times 10^{-3} \text{ cm}^{-1}$. A cooling device allows the electrolyte temperature to be kept in the range of [15 - 25 °C]. All the PEO treatments carried out in this study were conducted using a bipolar pulsed current generator working at 100 Hz within the so-called “soft-regime” corresponding to electrical conditions that are reported in detail in reference [3]. Within such a regime, the anodic (Q_p) to cathodic (Q_n) charge quantity ratio R is set at 0.89 ($R = Q_p / Q_n$) which greatly improves the

properties of the as-synthesized oxide layer. Indeed, detrimental effects caused by strong arc discharges are strongly reduced. The anodic and cathodic current amplitudes were steered at 30 A and -20 A respectively throughout each experiment. This corresponds to an anodic (resp. cathodic) current density of $76 \text{ A}\cdot\text{dm}^{-2}$ (resp. $-50.5 \text{ A}\cdot\text{dm}^{-2}$). Voltage-time and current-time responses were monitored using a 1 GHz bandwidth oscilloscope (Agilent 54832B) during the entire course of each PEO treatment.

The electrolyte consists of a solution of potassium hydroxide ($[\text{KOH}] = 1 \text{ g}\cdot\text{L}^{-1} \cong 0.018 \text{ mol}\cdot\text{L}^{-1}$) and anhydrous sodium silicate ($[\text{Na}_2\text{SiO}_3] = 1.65 \text{ g}\cdot\text{L}^{-1} \cong 0.014 \text{ mol}\cdot\text{L}^{-1}$) diluted in deionized water. It has been deliberately aged in this electrolyte during 8 hours by running the process in the same electrical conditions. Every hour, the aged sample recently treated was removed from the electrolysis tank, rinsed, dried and rapidly replaced with an untreated one. After each treatment, a 10 mL electrolyte sampling is operated for further chemical analyses.

Video images of the micro-discharges appearing during processing were recorded using a Photron SA1.1 camera which allows us to track the evolution of their characteristics either along the current period or over the processing time. Fast video recordings were synchronized with the current pulses. For the present study, only the lower half-part of the sample is filmed over an area of 7.5 cm^2 (see Fig. 1 a.). The sampling rate is set at 125 000 frames per second (125 kfps), which corresponds to a time resolution of $8 \mu\text{s}$. Within these specific sampling conditions, the spatial resolution of the camera was set at 0.017 mm^2 which is much lower (by a factor of ~ 15) than the minimum area of micro-discharges that was detected in the experiments. We resorted to automatic image processing by using a homemade software that provides the micro-discharge surface density per unit time, their lifetime (ms) and size (cross-sectional area in mm^2) distribution on the surface as a function of time [20].

Top views and cross-sections of the PEO-treated samples were examined by field emission gun scanning electron microscopy (FEG-SEM - Philips XL30) working in secondary and

backscattered electron mode, respectively. Chemical composition and distribution of elements in the synthesized oxide layers were determined by EDX analyses. Prior to be examined, samples were cut, mounted in resin, polished through successive grades of SiC abrasive papers and finely polished to 1 μm with diamond paste. The centre and the edge of the treated samples were closely examined as defined in Fig. 1 b. The central area of the sample is defined as an investigated area (2 mm \times 2 mm) centred at the intersection of the two diagonals of the rectangular shape of the sample while the edge area of the sample is located at 1 mm from the centre of its longest side. In both regions, the coating thickness was determined as the average value of 20 measures taken on cross-section over 20 different positions (each 100 μm). The average mean surface roughness of the coating, R_a (μm), was assessed using a Surfscan 3S profilometer with lateral and depth resolutions of 8 μm and 0.1 μm , respectively. The phase composition of the layer was investigated by X-ray diffraction measurements (XRD) using a Bruker D8 ADVANCE (Cu- $K_{\alpha 1}$ radiation $\lambda = 0.1542$ nm) instrument operated in Bragg-Brentano geometry with a step size of 0.005° and a scan range from 10 to 100° . XRD measurements were performed on the surface of the whole processed samples. The relative content of corundum phase (α - Al_2O_3) in the oxide layer was deduced from XRD peak adjustment and calculated from the integrated intensity of α - Al_2O_3 peaks compared with the integrated ones of both α - and η - Al_2O_3 .

At different stages of the ageing process, the electrical conductivity (σ_{el}) of the electrolyte solution was measured using a Hach SENSION conductimetre. The initial conductivity of the electrolyte, measured before the first PEO treatment, was $7.5 \text{ mS}\cdot\text{cm}^{-1}$. As a complement, changes in the ionic species amount in the electrolyte solution with the ageing process were evaluated using the Inductive Coupled Plasma – Atomic Emission Spectroscopy (ICP-AES) analytical technique. Analyses were particularly focused on the content variations of sodium

Na, potassium K and silicon Si ions, the three main components of the base electrolyte, and on the aluminium Al ions coming from the partial dissolution of the treated alloy.

3 Experimental results and discussion

3.1 Electrolyte characterization

The variation of the electrical conductivity versus the ageing time is shown in Fig. 2. After 1 hour, quite no significant change in the electrical properties is noted ($\sigma_{el} = 7.5 \text{ mS.cm}^{-1}$). Nevertheless, between 1 and 5 hours, a quasi-linear conductivity decrease occurs from 7.5 to 6.8 mS.cm^{-1} . After 5 hours effective use, the electrical conductivity of the electrolyte seems to keep a constant value at about 6.8 mS.cm^{-1} . Such changes in the electrical conductivity of the electrolyte are related to chemical changes in the content of dissolved species in the electrolyte. Table 1 lists the content of Na, K, Si and Al ionic species in the electrolyte determined by ICP-AES analysis after 1, 3 and 8 hours of effective use. The content of the base electrolyte elements (Na, K, Si) decreases as the electrolyte ages. Conversely the content of Al ionic species, that are initially absent from the fresh electrolyte, increases with the electrolyte duration of use. Therefore, the electrolyte is depleted in species coming from the potassium hydroxide KOH and sodium silicate Na_2SiO_3 solution while it is enriched in Al ionic species that are issued from the partial dissolution of the PEO treated aluminium samples. Note that changes in the ionic species content start to be noticeable only after 3 hours, for a rather small value of the active electrode area to electrolyte volume ratio ($1.6 \times 10^{-3} \text{ cm}^{-1}$).

3.2 Voltage-time responses

Fig. 3 shows the anodic voltage-time responses of the PEO treatments performed in three different aged electrolytes (1, 4 and 8 h). They reveal similar trends whatever the electrolyte age. From these responses, four successive stages can be distinguished. During the first stage (stage I), within a short period of time (about 10 s), a barrier-type anodic film develops on the surface by conventional anodizing mechanisms with a rapid increases in voltage amplitude ($\sim 40 \text{ V.s}^{-1}$) to keep the current constant. At this stage, no micro-discharges are observed while a bluish luminescence and an intense gas release are visible all over the sample surface. From 10 s on, the process suddenly enters a second stage (stage II). During this period that ranges from 10 s to around 13-20 min depending on the electrolyte ageing level, the slope of the voltage- time curve reduces to $\sim 0.04 \text{ V.s}^{-1}$. This change occurs at an anodic voltage value hereinafter referred to as the anodic breakdown voltage. Once this anodic breakdown voltage is reached ($\sim 750 \text{ V}$), small orange-red discharges initiate on the sample surface, preferentially at corners and edges of the sample. Fig. 3 shows that the electrolyte age has almost no influence, neither on the anodic breakdown voltage nor on the duration of stage II. The third stage (stage III) is characterized by an abrupt drop in the anodic voltage amplitude. This phenomenon was previously reported during AC PEO of aluminium in “soft” regime conditions [3]. This voltage transition is directly correlated with a change in the optical and acoustic characteristics of the discharges [21]. This voltage transition is also named “arcs” to “soft” regime transition because the micro-discharges progressively change to smaller size and shorter lifetime tiny discharges inducing less detrimental effects on the elaborated PEO layers [4]. Fig. 4 describes the evolution of the “arcs” to “soft” regime switching time as a function of the ageing time. The ageing of the electrolyte influences the development of the “soft” sparking regime since this regime appears earlier with an aged electrolyte. With the less aged electrolyte, the “soft” regime occurs gradually at $\sim 18 \text{ min}$, but almost instantaneously at

13 min with the older one. Finally, the fourth and ultimate stage of the PEO treatment (stage IV) is observed after about 20 min of processing time (Fig. 3). This stage consists of a constant and lower working voltage amplitude which depends on the ageing time. Indeed, Fig. 4 shows that anodic voltage amplitude is the highest at the beginning of the ageing process of the electrolyte (~ 710 V after 1 h of ageing), then it drops significantly between 2– and 4 h and it stabilizes to an almost constant value at ~ 640 V after 5 h.

3.3 Micro-discharges characteristics

Fig. 5 shows the spatial distributions of the micro-discharges over the processed surface at various times (1, 5 and 14 min). Each plot consists of 11250 processed images integrated over 9 periods of the current (90 ms). Figs. 5 a.-c. (resp. Figs. 5 d.-f.) present the spatial distributions recorded on the sample treated in the fresh electrolyte (resp. 8 h-aged electrolyte). Regardless of the state of the electrolyte, it clearly appears that the number of micro-discharges gradually decreases as the PEO process time increases. Such a decrease is more accentuated in the case of the 8 h-aged electrolyte. At 14 min, almost no visible micro-discharges are observed for the most aged electrolyte (Fig. 5 f.) while some discharges are actually detected in the less aged electrolyte, preferentially at the centre of the sample (Fig. 5 c.). This can be explained by considering the fact that the development of the “soft” sparking regime has occurred earlier for the aged electrolyte (at ~ 13 min) than for the fresh one (at ~ 20 min). Moreover, Fig. 5 also shows that samples are non-homogeneously covered by the micro-discharges. At the beginning of the process, micro-discharges are located around the corners and edges of the samples and then gradually, they cover the whole specimen area. This edge effect, which has been already reported in previous works [4, 21] occurs for all the

samples but it is slightly more pronounced for the sample processed in the fresh electrolyte (Fig. 5 b.) compared to the sample processed in the 8 h-aged electrolyte (Fig. 5 e.).

Fig. 6 depicts the time evolution of surface density of micro-discharges per second for three electrolytes aged for 1, 4 and 8 h. The inset highlights the influence of the ageing of the electrolyte during “arcs” regime (*i.e.* before the development of the “soft” sparking regime). Whatever the state of the electrolyte, the micro-discharge surface density per second at the beginning of stage II (between 10 s and 5 min) is higher than $3 \cdot 10^5 \text{ cm}^{-2} \cdot \text{s}^{-1}$. As the PEO process goes on, the surface density of micro-discharges per second decreases by more than one order of magnitude to reach an almost constant low value ($\sim 10^4 \text{ cm}^{-2} \cdot \text{s}^{-1}$) beyond 20 min, once the “soft” sparking regime is established. The inset of the Fig. 6 highlights that this decrease is much stronger at longer ageing times.

In Fig. 7, the time dependence of other characteristics of the micro-discharges (only during the “arcs” sparking regime) is depicted for various ageing times (1, 4 and 8 h), such as the size (Fig. 7 a.-c.) and the lifetime (Fig. 7 d.-f.) of individual micro-discharges. From size distributions, four categories of species can be distinguished: small, medium, large and very large micro-discharges with cross sectional areas in the ranges of $0.2 \pm 0.2 \text{ mm}^2$, $0.7 \pm 0.3 \text{ mm}^2$, $1.3 \pm 0.3 \text{ mm}^2$ and $>1.6 \text{ mm}^2$, respectively. Similarly, four categories of micro-discharges lifetime can be identified as short, medium, long and very long micro-discharges in the range of $0.02 \pm 0.02 \text{ ms}$, $0.07 \pm 0.03 \text{ ms}$, $0.15 \pm 0.05 \text{ ms}$ and $> 0.2 \text{ ms}$, respectively. At 1 min, (*i.e.* when the PEO process enters stage II), the behaviour of the micro-discharges is similar for the different investigated electrolytes. Indeed, no major differences are observed on the size and lifetime distributions between the sample processed in the fresh electrolyte and the other processed in aged electrolytes (Fig. 7 a. and d.). As the process enters the “arcs” sparking regime (stage III), the relative amount of large-size and long micro-discharges gradually increases. At 8 min, slight differences can be noticed between samples treated in

different electrolytes (Fig. 7 b. and e.) as smaller and shorter micro-discharges are detected in the aged electrolyte. At 14 min (*i.e.* at the end of the “arcs” sparking regime), such differences are more pronounced and easily visible. Indeed the population of micro-discharges with a very large size ($> 1.6 \text{ mm}^2$ cross-sectional area) is about 41, 4 and $1 \text{ cm}^{-2}.\text{s}^{-1}$ while that of long duration micro-discharges ($0.15 \pm 0.05 \text{ ms}$) is about 79, 6 and $0 \text{ cm}^{-2}.\text{s}^{-1}$ in the 1, 4 and 8h-aged electrolyte, respectively (Fig. 7 c. and f.). Then, results on the characterization of micro-discharges demonstrate that contrary to the fresh electrolyte, process in aged electrolytes promotes micro-discharges characterized by a smaller size and a shorter lifetime.

3.4 Discussion about the elaborated PEO coatings

Fig. 8 shows the backscattered cross-sectional SEM images of PEO oxide layers grown on Al2214 aluminium alloy. Micrographs were taken at the edge and at the centre of samples processed for one hour in the fresh (Fig. 8a.-b., respectively) and in the 8 h-aged electrolyte (Fig. 8c.-d., respectively). All the synthesized coatings exhibit two distinct regions that are characteristic of PEO layers elaborated in the “soft” regime conditions: a thick compact inner sublayer adjacent to aluminium substrate and a porous outer sublayer [3]. Regardless of the state of the electrolyte, micrographs evidence that the thickness is larger at the edge than at the centre. The homogeneity of the thickness is also improved at the edges where a smoother oxide layer / substrate interface is observed. This trend, already reported by Melhem *et al.* [21], has been explained recently by demonstrating that the occurrence of the “soft” regime is spatially deferred [4]. Indeed, this regime occurs earlier at corners and edges and then propagates towards the centre which suffers the detrimental “arcs” regime a longer time. Moreover, micrographs evidence that using a fresh electrolyte leads to thicker oxide layers.

This is even more obvious at the centre. Nevertheless, micrographs also show that proportion of the porous outer sublayer in the total coating thickness is larger when a fresh electrolyte is used. The aspect of the topmost surface of the coating elaborated in the fresh electrolyte is more irregular and rugged than that synthesized in the 8 h-aged electrolyte. Residual discharge channels are even visible at the topmost surface of the coating formed in the fresh electrolyte.

From cross-sectional SEM micrographs, average thicknesses of oxide layers were determined at the edge and at the centre. Fig. 9 depicts the thickness variation of the total and outer sublayer as a function of the ageing time of the electrolyte. As previously noted (Fig. 8), the thickness of the total layer is always larger at the edge than at the centre whatever the state of the electrolyte. For the fresh one, the total layer thickness is about 120 μm at the edge and about 95 μm at the centre. Concerning the thickness of the porous outer sublayer, no significant differences were noted between edge and centre. Within the range of the operating conditions used in this study, ageing of the PEO electrolyte has a distinct influence on the oxide coating thickness. Indeed, wherever on the sample, the thickness of the overall oxide layer decreases with the ageing time. It is also noteworthy that this trend is more pronounced at the centre than at the edge, suggesting that fresh electrolyte minimizes the spatial heterogeneity of the coating thickness over the processed surface. Nevertheless, even if the improvement in the overall layer thickness with fresh electrolytes is effective, Fig. 9 also shows that the use of such a fresh electrolyte results in an increase in the thickness of the outer porous sublayer, which is known to give poor mechanical properties and disastrous corrosion resistance [22]. At the edge of the samples, the proportion of the outer sublayer is about 30 % of the total layer thickness for a fresh electrolyte but only 13 % for a 8 h-aged electrolyte.

Fig. 10 shows the top view macrographs of half a sample treated for one hour in a fresh electrolyte (Fig. 10 a.) and in the 8 h-aged one (Fig. 10 b.). Dark dots are clearly visible on the surface of the sample processed in the fresh electrolyte. They are preferentially located at edges. Such defaults on the surface are large open pores ($\sim 100 - 300 \mu\text{m}$ in diameter) and correspond to discharge channels. This observation is correlated with the “arcs” regime previously described. Indeed, as already mentioned, the population of long-duration and large-size micro-discharges is larger for the fresh electrolyte than for the 8 h-aged one, suggesting a more damaged surface with large open pores all over the surface.

Fig. 11 shows the 3D surface topography measured with a touch probe carried out at the edge of the samples processed for one hour in a fresh electrolyte (Fig. 11 a.) and in an 8 h-aged electrolyte (Fig. 11 b.). The surface of the oxide layer synthesized in the fresh electrolyte is rougher. Deep pits are found on the scanned surface that matches with defaults observed previously in Fig. 10 a. From surface topographies in Fig. 11, the roughness parameter R_a (the arithmetic mean value) was calculated at both the edge and the centre of each processed sample of this study. Fig. 12 shows the variation of R_a as a function of the ageing time of the PEO electrolyte. The roughness value at the centre of the samples is always lower than the one at the edge, whatever the state of the electrolyte. This corroborates macroscopic observations made on the samples presented in Fig. 10 where large defaults and open porosities are preferentially localized at edges. Moreover, Fig. 12 also evidences that R_a decreases with the ageing time of the electrolyte. For example, at the centre of the samples, R_a value is about $5 \mu\text{m}$ with the fresh electrolyte and decreases to about $3.5 \mu\text{m}$ with the most aged electrolyte. The surface becomes smoother as the electrolyte gets aged. Such a decrease in the surface roughness is much more pronounced after 2 hours while after 5 hours, R_a stands at a low and almost constant value.

Fig. 13 presents the secondary electrons SEM top view micrographs showing the surface of the layers grown on Al2214 aluminium alloy. Micrographs were taken at the edge and at the centre of samples processed for one hour in the fresh (Fig. 13 a.-b., respectively) and in the 8 h-aged electrolyte (Fig. 13 c.-d., respectively). Surfaces exhibit a typical morphology of PEO coatings with a mixture of “pancake”-like structures (site “A” in Fig. 13 b.) surrounded by and filled with “sponge”-like structures (site “B” in Fig. 13 d.). The presence of “pancake” is a typical feature of PEO layers grown on aluminium in “arcs” regime conditions. Such layers are characterized by a micro-porosity which diameter size ranges from 5 to 20 μm . In contrast, the presence of “sponges” characterized by sharp pores (typ. 0.1 to 1 μm in diameter) is usually a footprint of aluminium substrates processed in “soft” regime conditions [3,4, 21]. This “sponge”-like structure is also known to contain silicon [23]. Fig 13 shows that the surface of the oxide coating elaborated in the fresh electrolyte is largely dominated by “pancakes” surrounded by a few “sponges”. In contrast, by using the most aged electrolyte, “sponges” are interconnected and cover the whole surface of the layer. Such an observation can be explained by the earlier development of the “soft” regime when the electrolyte is aged, the sample surface being thus much longer submitted to the “soft” regime.

Fig. 14 shows the EDX spectra recorded on the topmost surface (*i.e.* the outer sublayer) of the PEO coatings elaborated in 1, 4 and 8 h-aged electrolytes. Note that the surface area analyzed is about 900 μm^2 (square of size 30 μm \times 30 μm). The outer sublayer contains Al, Mg, Cu, O, Si, Na, K, C and Au regardless of the state of the electrolyte. Note that Al, Mg and Cu come from the Al2214 alloy substrate while O, Si, Na, and K come from the electrolyte (*i.e.* from potassium hydroxide KOH and sodium silicate Na_2SiO_3 dissolved in deionised water). Detection of C and Au are due to traces of organic impurities and gold metallisation required to enhance SEM observations. The proportion of O and Al in the outer sublayer of the PEO coatings remains almost constant whatever the state of the electrolyte. In contrast, EDX

spectra show an increase in the amount of Na, Si and K species contained in the outer sublayer with the increase in ageing time of the electrolyte. This result is consistent with previous SEM observations (Fig. 13) showing that the “sponge”-like structures, which are well-known to incorporate elements from the electrolyte, are denser with an aged electrolyte [23-26]. Moreover, this progressive enrichment of the outer sublayer could explain to some extent the progressive depletion of the ionic species as assessed previously by ICP-AES (see Table 1). Further investigations should however be conducted to get confirmation of this assumption.

Fig. 15 presents EDX maps of Al, O, Si, Na, and K distributions throughout the total layers synthesized in the fresh electrolyte (column a. in Fig. 15) and in an 8 h-aged electrolyte (column b. in Fig. 15). In addition to the former EDX information, these maps evidence that Si, K and Na species are preferentially located in the outer porous sublayers of the coatings, regardless of the age of the electrolyte, while the inner sublayer is mainly composed of Al and O. Nevertheless, some differences are observed between layers grown in the two electrolytes. In the case of the fresh one, Si, K and Na are non-evenly distributed throughout the outer sublayer and some traces are also found in the inner sublayer. This is particularly true for Na. In contrast, these three elements are localized only throughout the outer sublayer of the coating grown in the 8 h-old electrolyte. Moreover, Fig. 15 shows that Cu, initially present in the substrate as the main alloying element, forms an interconnected network exclusively distributed throughout the inner sublayer. Concerning the distribution of this element, no differences are noted between the samples processed in either electrolyte.

The X-ray diffraction patterns of the PEO layers grown for 1 h in various aged electrolytes (1, 4 and 8 h) are depicted in Fig. 16. All coatings are predominantly composed of α - and η -phases of crystalline alumina Al_2O_3 . A weak and broad bump centred at $30\text{-}40^\circ$ is assigned to the presence of an amorphous phase in the outer part of the oxide layer, possibly made of

amorphous silica SiO_2 or aluminosilica $3(\text{AlO}_3)\cdot 2(\text{SiO}_2)$, as suggested by the spatial distribution of Si throughout the oxide layer (Fig. 15). In Fig. 16, the appearance of aluminium peaks is due to the diagnostic method based on the use of incident X-ray beam that cross entirely the PEO coating and reaches the aluminium substrate. The peaks of cuprite Cu_2O , which overlap those of $\eta\text{-Al}_2\text{O}_3$ have been identified. Oxidation of copper, the main alloying element of Al2214 aluminium alloys, does take place during the process. Combined with EDX maps in Fig. 15, XRD results suggest the presence of an inter-connected network of cuprite exclusively located in the inner part of the oxide layers.

Fig. 17 shows a selected region of XRD patterns in the range of $43\text{-}47^\circ$. Some authors have proposed to use the relative intensity of (113) $\alpha\text{-Al}_2\text{O}_3$ (at 43.6°) and (400) $\eta\text{-Al}_2\text{O}_3$ (at 45.96°) peaks to judge on the α - and η -alumina content and variations in the overall layer phase composition [27, 28]. Fig. 17 shows that such a relative intensity of α - and η -alumina peaks increases noticeably with the electrolyte ageing, suggesting an increase in the proportion of the α phase at the expense of the η one as the electrolyte gets aged. The relative content of $\alpha\text{-Al}_2\text{O}_3$ in the coating has been quantified for samples processed in various aged electrolytes. Fig. 18 reports the variation of the $\alpha\text{-Al}_2\text{O}_3$ content together with the variation of the intensity ratio $(113)_\alpha/(400)_\eta$ as a function of the ageing time of the electrolyte. First of all, a strong correlation is observed between the variation of the calculated $\alpha\text{-Al}_2\text{O}_3$ content and the variation of the intensity ratio $(113)_\alpha/(400)_\eta$. It supports the idea of using the intensity ratio $(113)_\alpha / (400)_\eta$ to describe the proportions of α - and $\eta\text{-Al}_2\text{O}_3$ phases in the layer. Fig. 18 also shows that the $\alpha\text{-Al}_2\text{O}_3$ content is always lower than 50 %. This agrees with the widely-reported conclusion that, in PEO layers grown on aluminium alloys, the η -alumina phase is the main crystalline phase. Moreover, Fig. 17 evidences the influence of the ageing process of the electrolyte on the phase composition of the synthesized layers. Indeed, the $\alpha\text{-Al}_2\text{O}_3$

content increases with the ageing time of the electrolyte. With the fresh electrolyte, the α - Al_2O_3 content is about 36 % while it reaches about 43 % with the most-aged electrolyte. This trend can be explained by the earlier development of the “soft” regime as the electrolyte gets aged (see Fig. 4), this regime being known to promote the growth of the α - Al_2O_3 phase [18,29, 30]. Moreover, the change in the α - Al_2O_3 increase rate after 2 hours ageing suggests that ageing of the electrolyte is effective after about 2 -3 hours of processing. This result is in good agreement with those obtained previously with chemical analysis of the electrolyte, fast video-imaging and coating morphology characterization.

4. Conclusion

In this study, evidence and influence of ageing of the electrolyte on Plasma Electrolytic Oxidation (PEO) of Al2214 aluminium alloy has been investigated with the use of various experimental techniques including fast-video imaging, chemical analysis and material science. The tested electrolyte ($\text{KOH}+\text{Na}_2\text{SiO}_3$) has been deliberately aged during several hours. Cross-checked results support the same conclusion: chemical ageing of the PEO electrolyte occurs and alteration becomes effective after 2–3 h. of processing. The progressive depletion in the dissolved species (Na, K and Si) with the ageing of the electrolyte is responsible for the decrease in the electrical conductivity of the electrolyte. Ageing affects the oxide layer characteristics whose thickness becomes thinner and more compact with a reduced outer porous sublayer. In an aged electrolyte, the formation of an amorphous alumina-silicate barrier rich in elements coming from the electrolyte (Na, K and Si) that located throughout the outer sublayer is promoted together with the development of the crystalline α - Al_2O_3 alumina in the inner sublayer. Changes in the material are related to changes in the micro-discharges behaviour. As the PEO electrolyte gets aged, the beneficial “soft” oxidation regime appears

earlier, leading to less micro-discharges over the processed surface with smaller sizes and shorter lifetime.

Acknowledgements

We greatly acknowledge the Conseil Régional de Lorraine for granting A. Nominé's PhD work under decision 11CP-769. We are also deeply grateful to the FONGECIF Rhône-Alpes for granting P. Leone's graduate school internship. This work was supported by the French Government through the program "Investissements d'avenir" operated by the French National Research Agency (ANR) and referenced to as ANR-11-LABX-0008-01 (LabEx DAMAS).

List of references

- [1] A.L. Yerokhin, X. Nie, A. Leyland, A. Matthews, S.J. Dowey, *Surf. Coat. Technol.* 122 (1999) 73-93.
- [2] E. Matykina, A. Berkani, P. Skeldon, G.E. Thompson, *Electrochim. Acta* 53 (2007) 1987-1994.
- [3] F. Jaspard-Mécuson, T. Czerwiec, G. Henrion, T. Belmonte, L. Dujardin, A. Viola, J. Beauvir, *Surf. Coat. Technol.* 201 (2007) 8677-8682.
- [4] J. Martin, A. Melhem, I. Shchedrina, T. Duchanoy, A. Nominé, G. Henrion, T. Czerwiec, T. Belmonte, *Surf. Coat. Technol.* 221 (2013) 70-76
- [5] L.O. Snizhko, A.L. Yerokhin, A. Pilkington, N.L. Gurevina, D.O. Misnyankin, A. Leyland, A. Matthews, *Electrochim. Acta* 49 (2004) 2085-2095
- [6] A.A. Voevodin, A.L. Yerokhin, V.V. Lyubimov, M.S. Donley, J.S. Zabinski, *Surf. Coat. Technol.* 86-87 (1996) 516-521.
- [7] P. Bala Srinivasan, J. Liang, R.G. Balajee, C. Blawert, M. Störmer, W. Dietzel, *Appl. Surf. Sci.* 256 (2010) 3928-3935.
- [8] J.A. Curran, H. Kalkanci, Yu. Magurova, T.W. Clyne, *Surf. Coat. Technol.* 201 (2007) 8683-8687
- [9] F. Monfort, A. Berkani, E. Matykina, P. Skeldon, G.E. Thompson, H. Habazaki, K. Shimizu, *Corros. Sci.* 49 (2007) 672-693
- [10] H. Duan, C. Yan, F. Wang, *Electrochim. Acta* 52 (2007) 3785-3793
- [11] J. Liang, P. Bala Srinivasan, C. Blawert, M. Störmer, W. Dietzel, *Electrochim. Acta* 54 (2009) 3842-3850
- [12] R. Arrabal, E. Matykina, F. Viejo, P. Skeldon, G.E. Thompson, *Corros. Sci.* 50 (2008) 1744-1752

- [13] A. Ghasemi, V.S. Raja, C. Blawert, W. Dietzel, K.U. Kainer, *Surf. Coat. Technol.* 202 (2008) 3513-3518
- [14] A. Nemcova, P. Skeldon, G.E. Thompson, B. Pacal, *Surf. Coat. Technol.* 232 (2013) 827-838
- [15] P.I. Butyagin, Ye. V. Khokhryakov, A.I. Mamaev, *Mater. Lett.* 57 (2003) 1748-1751
- [16] J. Liang, L. Hu, J. Hao, *Electrochim. Acta* 52 (2007) 4836-4840
- [17] R. Arrabal, E. Matykina, F. Viejo, P. Skeldon, G.E. Thompson, M.C. Merino, *Appl. Surf. Sci.* 254 (2008) 6937-6942
- [18] E. Matykina, R. Arrabal, P. Skeldon, G.E. Thompson, *J. Appl. Electrochem.* 38 (2008) 1375-1383
- [19] O.P. Terleeva, A.I. Slonova, V.I. Belevantsev, I.B. Kireenko, A.P. Ryzikh, *Prot. Met. Phys. Chem. Surf.* 47 (2011) 80-85
- [20] S. Bardin, J-L. Briançon, F. Brochard, V. Martin, Y. Zayachuk, R. Hugon, J. Bougdira, *Contrib. Plasma Phys.* 51 (2011) 246-251.
- [21] A. Melhem, G. Henrion, T. Czerwiec, J.L. Briançon, T. Duchanoy, F. Brochard, T. Belmonte, *Surf. Coat. Technol.* 205 (2011) S133-S136.
- [22] R.C. Barik, J.A. Wharton, R.J.K. Wood, K.R. Stokes, R.L. Jones, *Surf. Coat. Technol.* 199 (2005) 158-167
- [23] Y-L. Cheng, Z-G. Xue, Q. Wang, X-Q. Wu, E. Matykina, P. Skeldon, G.G. Thompson, *Electrochim. Acta* 107 (2013) 358-378
- [24] V. Dehnavi, B.L. Luan, D.W. Shoesmith, X.Y. Liu, S. Rohani, *Surf. Coat. Technol.* 226 (2013) 100-107
- [25] R.O. Hussein, X. Nie, D.O. Northwood, A.L. Yerokhin, A. Matthews, *J. Phys. D: App. Phys.* 43 (2010) 105203
- [26] R.O. Hussein, X. Nie, D.O. Northwood, *Surf. Coat. Technol.* 205 (2010) 1659-1667

- [27] W. Xue, Zh Deng, Y. Lai, R. Chen, *J. Am. Ceram. Soc.* 81 (1998) 1365-1368
- [28] A.L. Yerokhin L.O. Snizhko, N.L. Gurevina, A. Leyland, A. Pilkington, A. Matthews, *J. Phys. D: Appl. Phys.* 36 (2003) 2110-2120
- [29] E. Matykina, R. Arrabal, P. Skeldon, G.E. Thompson, P. Belenguer, *Surf. Coat. Technol.* 205 (2010) 1668-1678
- [30] K. Tillous, T. Toll-Duchanoy, E. Bauer-Grosse, L. Hericher, G. Geandier, *Surf. Coat. Technol.* 203 (2009) 2969-2973

List of figure captions

Fig. 1. Schematic representation of the processed sample showing (a) the area filmed by fast video imaging and (b) the localization of the investigated central and edge area (2 mm × 2 mm)

Fig. 2. Variation of the electrical conductivity σ_{el} as a function of the ageing time of the electrolyte.

Fig. 3. Evolutions of the anodic voltage amplitude as a function of the PEO processing time in an electrolyte aged for 1h, 4h and 8h. The inset shows an expanded view of stage I.

Fig. 4. Variations of the “arcs -to -soft” regime switching time and the anodic voltage amplitude as a function of the ageing time of the electrolyte.

Fig. 5. Pictures of the spatial distribution of micro-discharges over the processed surface at three different processing times (1 min, 5 min and 14 min) in a fresh (pictures a., b. and c., respectively) and in an 8 h-aged electrolyte (pictures d., e. and f., respectively). Each picture corresponds to the integration of 11250 successive images recorded over 90 ms (9 current pulse periods).

Fig. 6. Evolutions of the micro-discharges surface number density per second with the PEO processing time for various ageing time of the electrolyte (1, 4 and 8 h). The figure inset highlights these evolutions before the development of the “soft” sparking regime.

Fig. 7. Size (a.-c.) and lifetime (d.-f.) distributions of micro-discharges recorded at three different processing times (1, 8 and 14 min) for various ageing time of the electrolyte (1, 4 and 8 h).

Fig. 8. Backscattered SEM micrographs of cross-sections of one-hour PEO processed samples in: (a) fresh electrolyte – at the edge of the sample, (b) fresh electrolyte – at the centre of the sample, (c) 8 h-aged electrolyte – at the edge of the sample and (d) 8 h-aged electrolyte – at the centre of the sample.

Fig. 9. Variations of the average total thickness (close symbols) and porous outer sublayer thickness (open symbols) of the PEO coatings (measured at the edge and at the centre of the processed samples) as a function of the ageing time of the electrolyte.

Fig. 10. Top view macrographs of the PEO treated samples (one half only) in a fresh (a) and in a 8 h-aged (b) electrolyte after one hour of processing time.

Fig. 11. 3-dimensional images of the surface topography of the PEO coatings formed in a fresh (a) and in a 8 h-aged (b) electrolyte after one hour of processing time. Measurements were carried out at the edge of the processed samples.

Fig. 12. Variations of the roughness parameter R_a (μm) measured at the edge and at the centre of the processed samples as a function of the ageing time of the electrolyte.

Fig. 13. Top view scanning electron micrographs (secondary electrons) of the surface of one-hour PEO processed samples in : (a) fresh electrolyte – at the edge of the sample, (b) fresh electrolyte – at the centre of the sample, (c) 8 h-aged electrolyte – at the edge of the sample and (d) 8 h-aged electrolyte – at the centre of the sample.

Fig. 14. EDX spectra recorded on the topmost surface of the PEO layers grown in an electrolyte aged for various times (1, 4 and 8 h). Measurements were carried out at the edge of the processed samples.

Fig. 15. Scanning electron micrographs and EDX element maps (Si, K and Na) of the cross-section of the PEO layers grown in a fresh (column a) and in a 8 h-aged (column b) electrolyte after one hour of processing time. Measurements were carried out at the edge of the processed samples.

Fig. 16. XRD patterns (using Bragg-Brentano geometry) of the PEO coatings synthesized for 1 hour in various aged electrolytes: (a) 1 h, (b) 4 h and (c) 8 h.

Fig. 17. Selected region of XRD patterns where (113) $\alpha\text{-Al}_2\text{O}_3$ and (400) $\eta\text{-Al}_2\text{O}_3$ peaks are found. Same conditions as in Fig. 16.

Fig. 18. Variation of the $\alpha\text{-Al}_2\text{O}_3$ content in the PEO layers (calculated from XRD measurements carried out at the centre of the processed samples) and variation of the intensity

ratio $(113)_\alpha / (400)_\eta$ of $(113) \alpha\text{-Al}_2\text{O}_3$ and $(400) \eta\text{-Al}_2\text{O}_3$ peaks as a function of the ageing time of the electrolyte.

List of tables

Table 1

Sodium, potassium, silicon and aluminium ionic species content into a 1 g.L⁻¹ KOH – 1.65 g.L⁻¹ Na₂SiO₃ PEO electrolyte after 1, 3 and 8 hours effective processing duration.

| Ageing time | Na | K | Si | Al |
|-------------|-------------------|-------------------|-------------------|-------------------|
| h | g.L ⁻¹ | g.L ⁻¹ | g.L ⁻¹ | g.L ⁻¹ |
| 1 | 0.120 | 0.549 | 0.385 | 0.007 |
| 3 | 0.120 | 0.539 | 0.367 | 0.015 |
| 8 | 0.116 | 0.505 | 0.317 | 0.047 |

List of figures

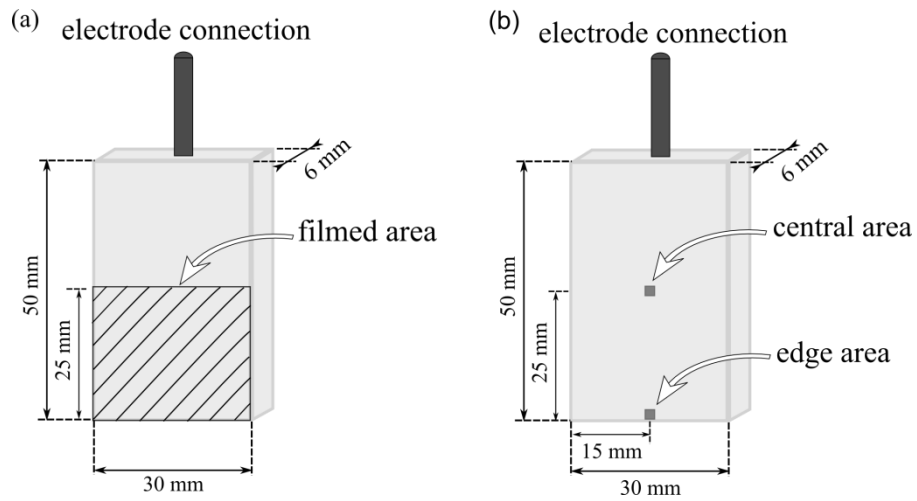


Fig. 1. Schematic representation of the processed sample showing (a) the area filmed by fast video imaging and (b) the localization of the investigated central and edge area (2 mm × 2 mm)

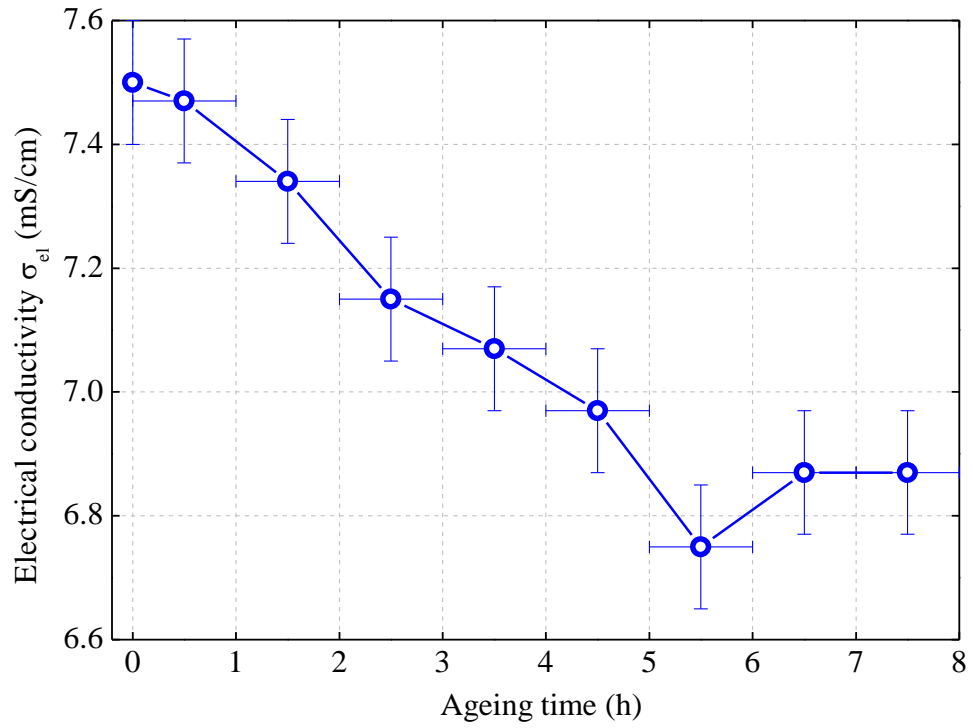


Fig. 2. Variation of the electrical conductivity σ_{el} as a function of the ageing time of the electrolyte.

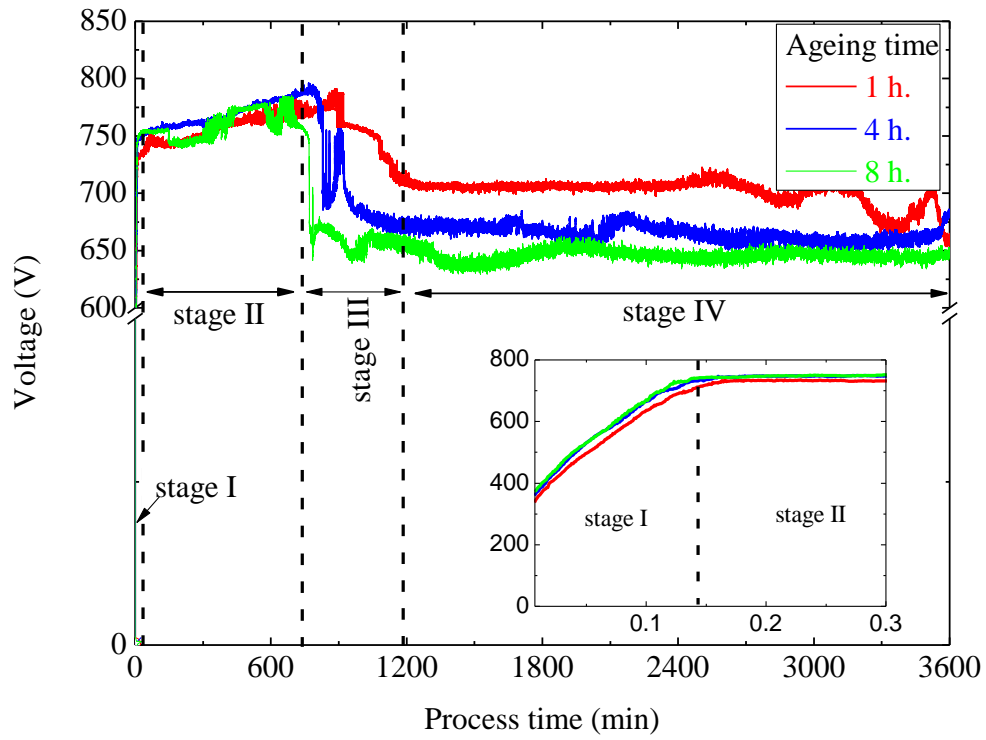


Fig. 3. Evolutions of the anodic voltage amplitude as a function of the PEO processing time in an electrolyte aged for 1h, 4h and 8h. The inset shows an expanded view of stage I.

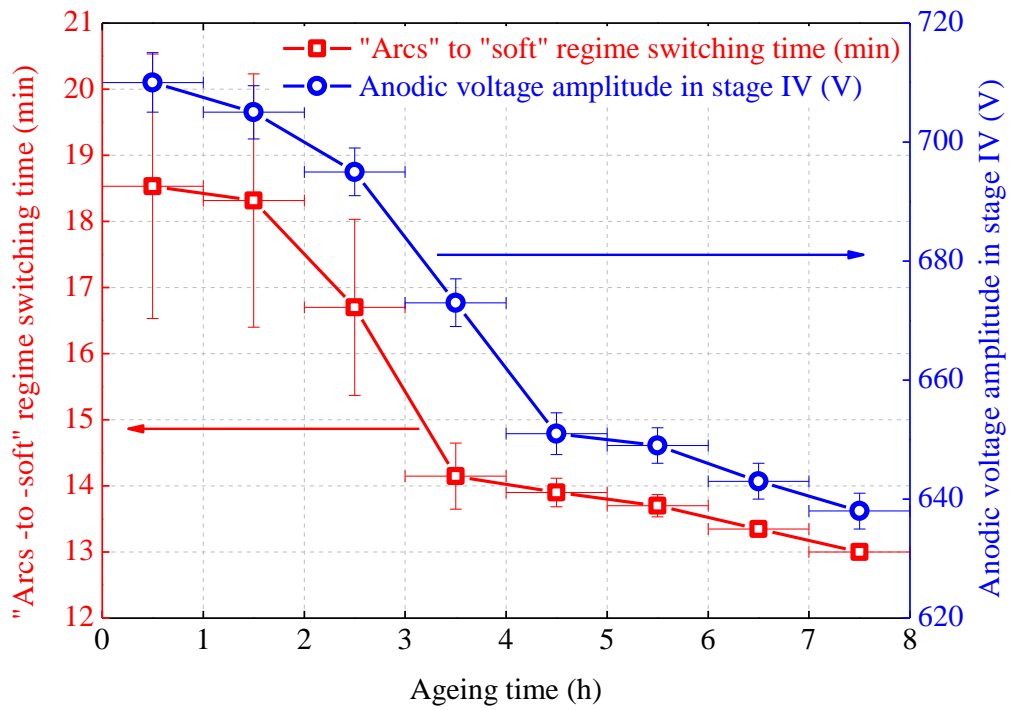


Fig. 4. Variations of the “arcs -to -soft” regime switching time and the anodic voltage amplitude as a function of the ageing time of the electrolyte.

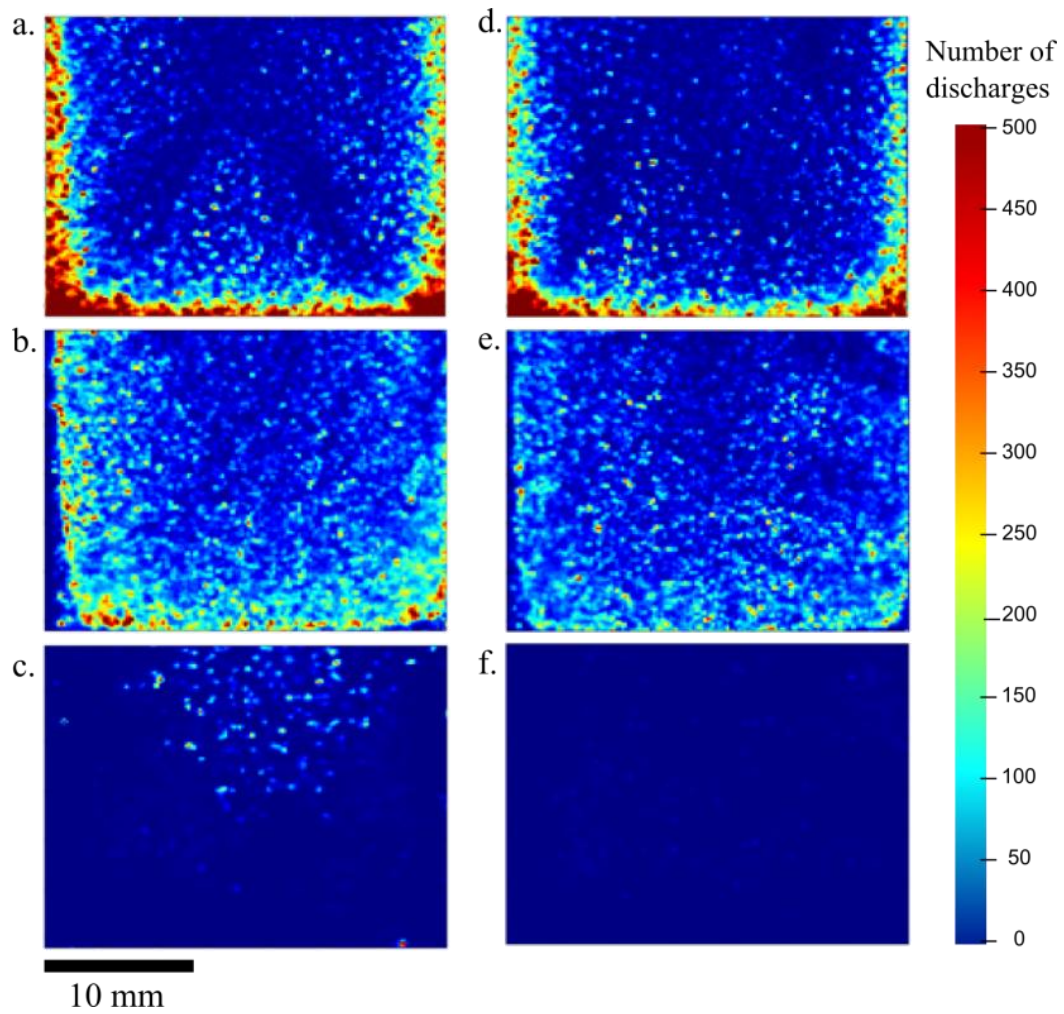


Fig. 5. Pictures of the spatial distribution of micro-discharges over the processed surface at three different processing times (1 min, 5 min and 14 min) in a fresh (pictures a., b. and c., respectively) and in an 8 h-aged electrolyte (pictures d., e. and f., respectively). Each picture corresponds to the integration of 11250 successive images recorded over 90 ms (9 current pulse periods).

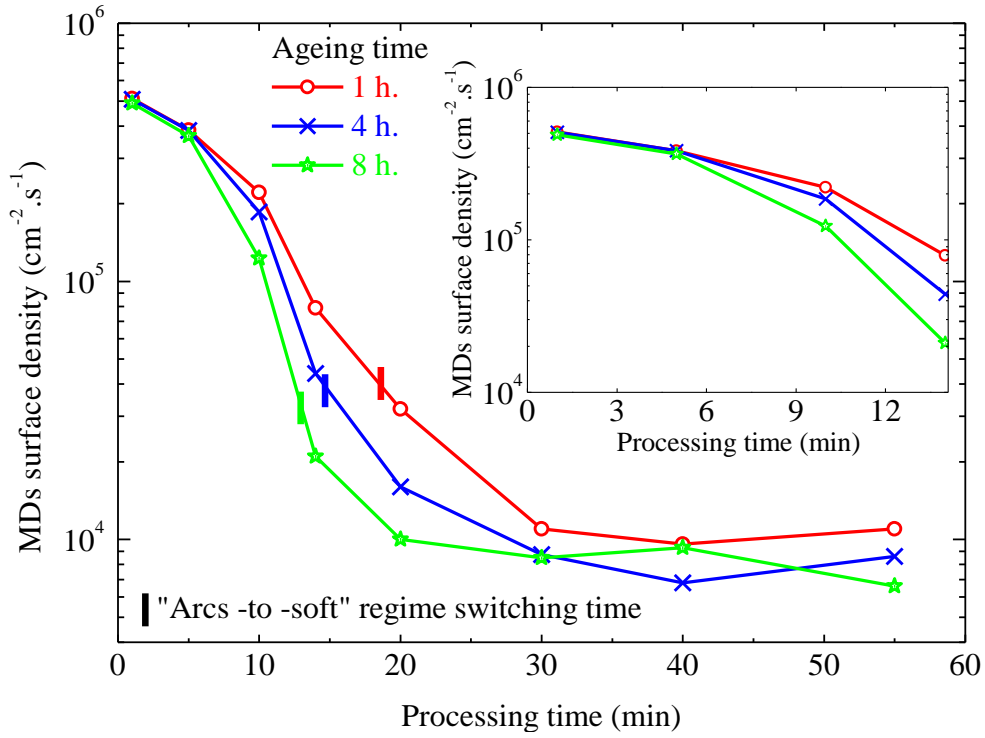


Fig. 6. Evolutions of the micro-discharges surface number density per second with the PEO processing time for various ageing time of the electrolyte (1, 4 and 8 h). The figure inset highlights these evolutions before the development of the “soft” sparking regime.

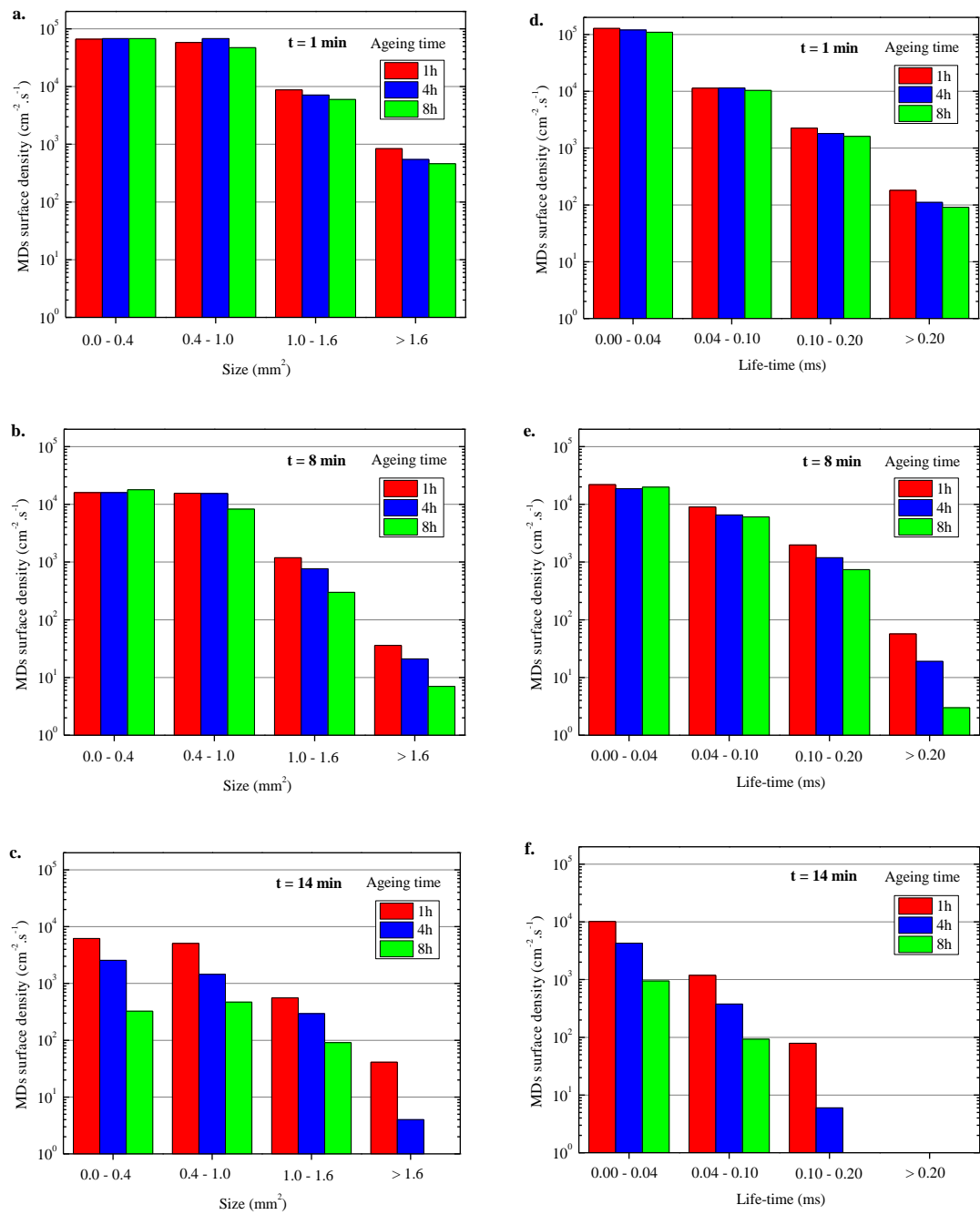


Fig. 7. Size (a.-c.) and lifetime (d.-f.) distributions of micro-discharges recorded at three different processing times (1, 8 and 14 min) for various ageing time of the electrolyte (1, 4 and 8 h).

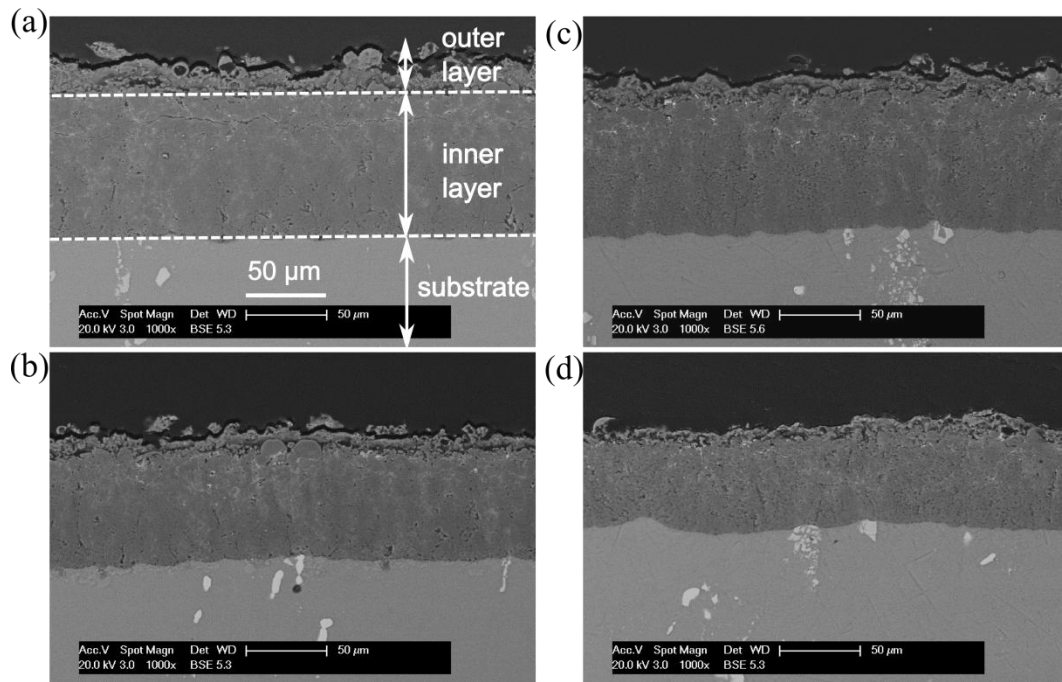


Fig. 8. Backscattered SEM micrographs of cross-sections of one-hour PEO processed samples in: (a) fresh electrolyte – at the edge of the sample, (b) fresh electrolyte – at the centre of the sample, (c) 8 h-aged electrolyte – at the edge of the sample and (d) 8 h-aged electrolyte – at the centre of the sample.

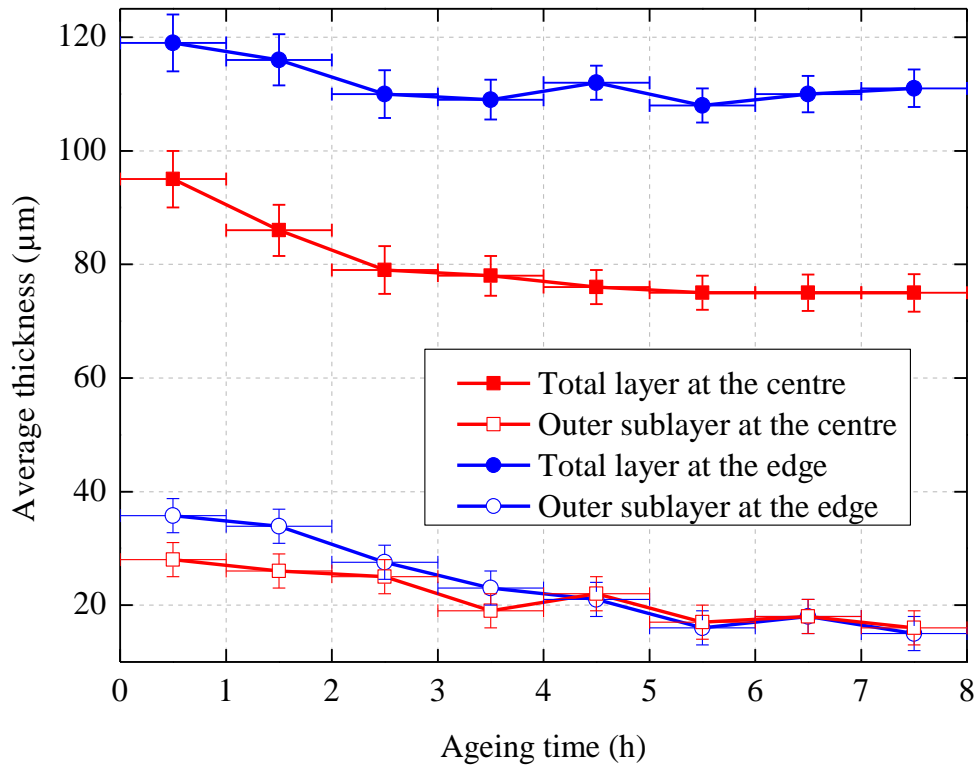


Fig. 9. Variations of the average total thickness (close symbols) and porous outer sublayer thickness (open symbols) of the PEO coatings (measured at the edge and at the centre of the processed samples) as a function of the ageing time of the electrolyte.

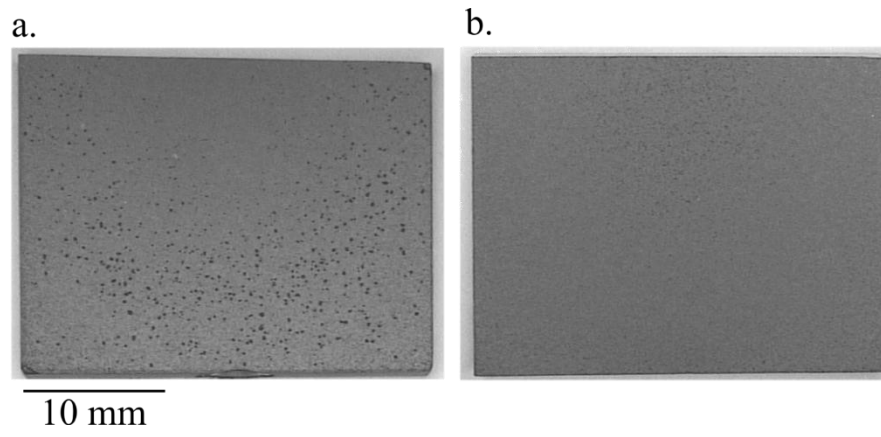


Fig. 10. Top view macrographs of the PEO treated samples (one half only) in a fresh (a.) and in a 8 h-aged (b.) electrolyte after one hour of processing time.

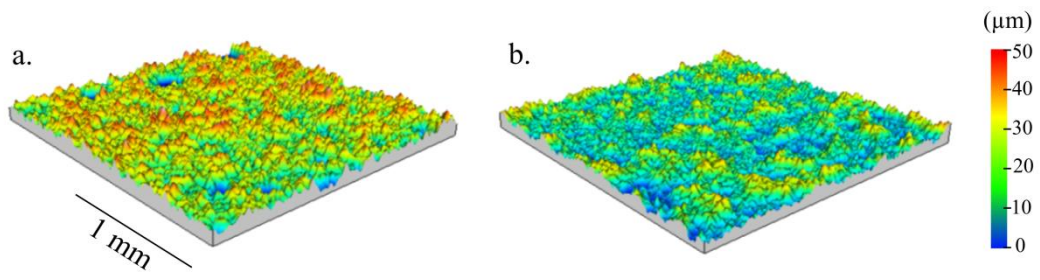


Fig. 11. 3-dimensional images of the surface topography of the PEO coatings formed in a fresh (a) and in a 8 h-aged (b) electrolyte after one hour of processing time. Measurements were carried out at the edge of the processed samples.

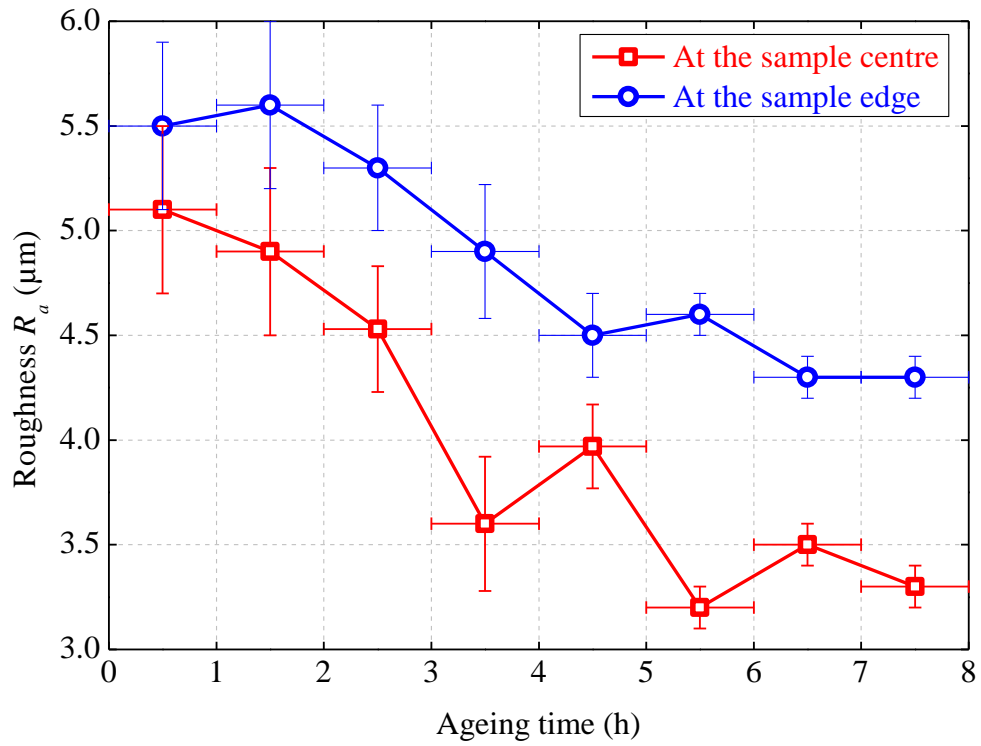


Fig. 12. Variations of the roughness parameter R_a (μm) measured at the edge and at the centre of the processed samples as a function of the ageing time of the electrolyte.

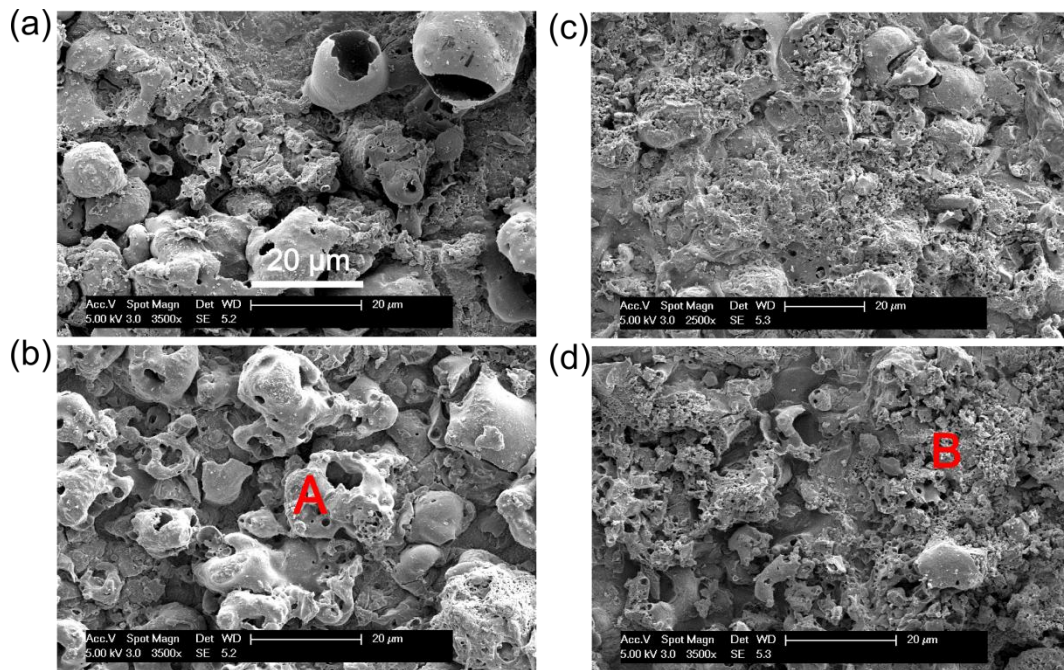


Fig. 13. Top view scanning electron micrographs (secondary electrons) of the surface of one-hour PEO processed samples in : (a) fresh electrolyte – at the edge of the sample, (b) fresh electrolyte – at the centre of the sample, (c) 8 h-aged electrolyte – at the edge of the sample and (d) 8 h-aged electrolyte – at the centre of the sample.

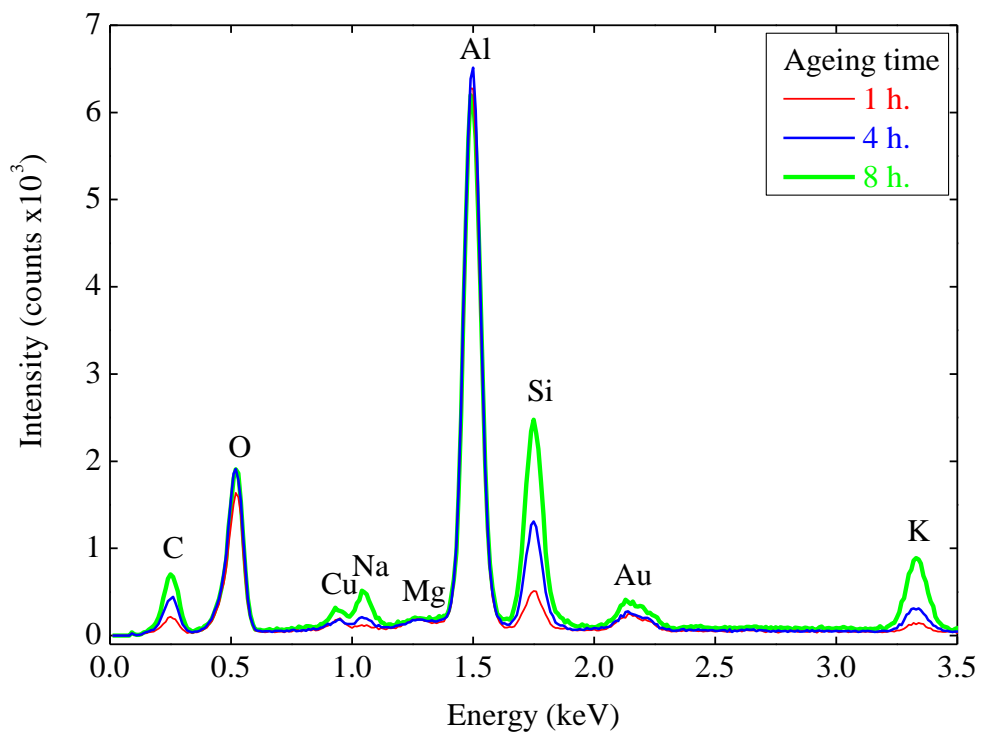


Fig. 14. EDX spectra recorded on the topmost surface of the PEO layers grown in an electrolyte aged for various times (1, 4 and 8 h). Measurements were carried out at the edge of the processed samples.

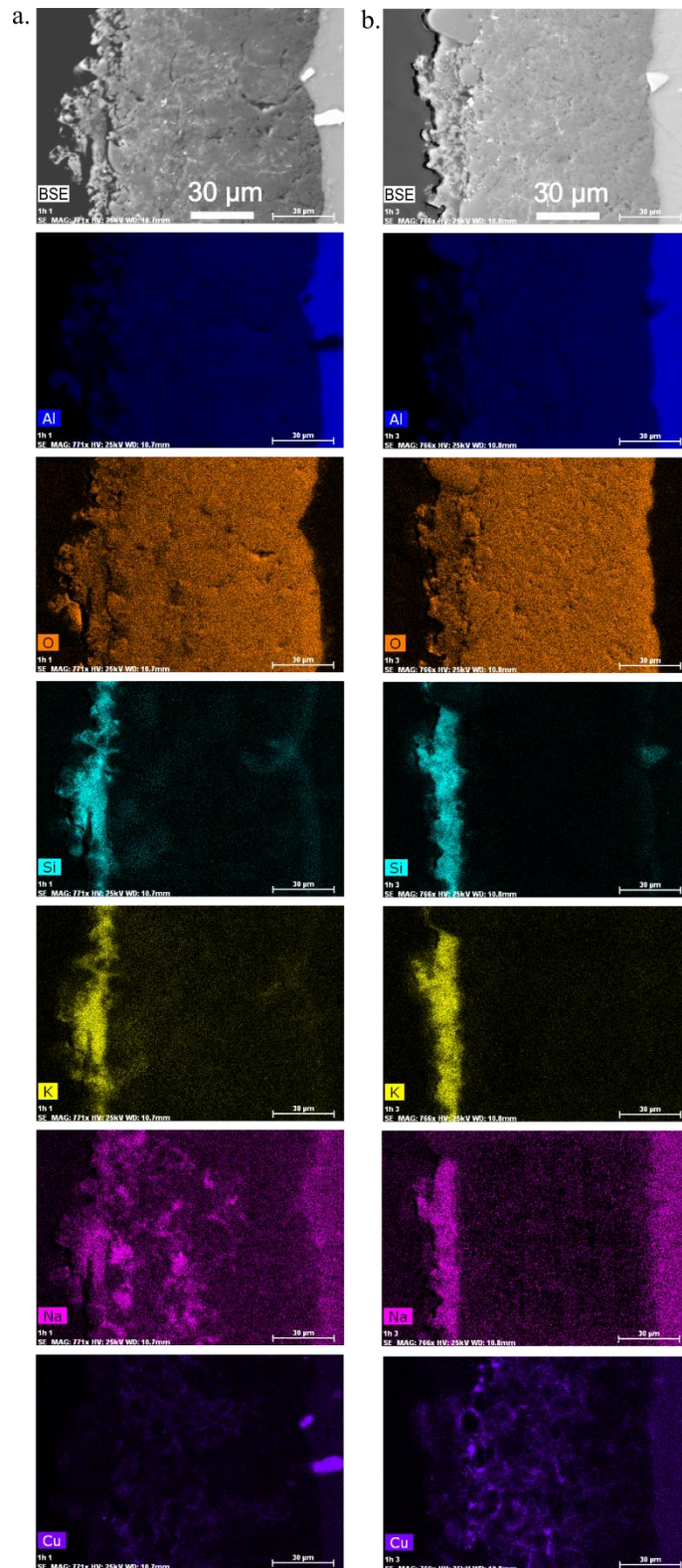


Fig. 15. Scanning electron micrographs and EDX element maps (Si, K and Na) of the cross-section of the PEO layers grown in a fresh (column a.) and in a 8 h-aged (column b.) electrolyte after one hour of processing time. Measurements were carried out at the edge of the processed samples.

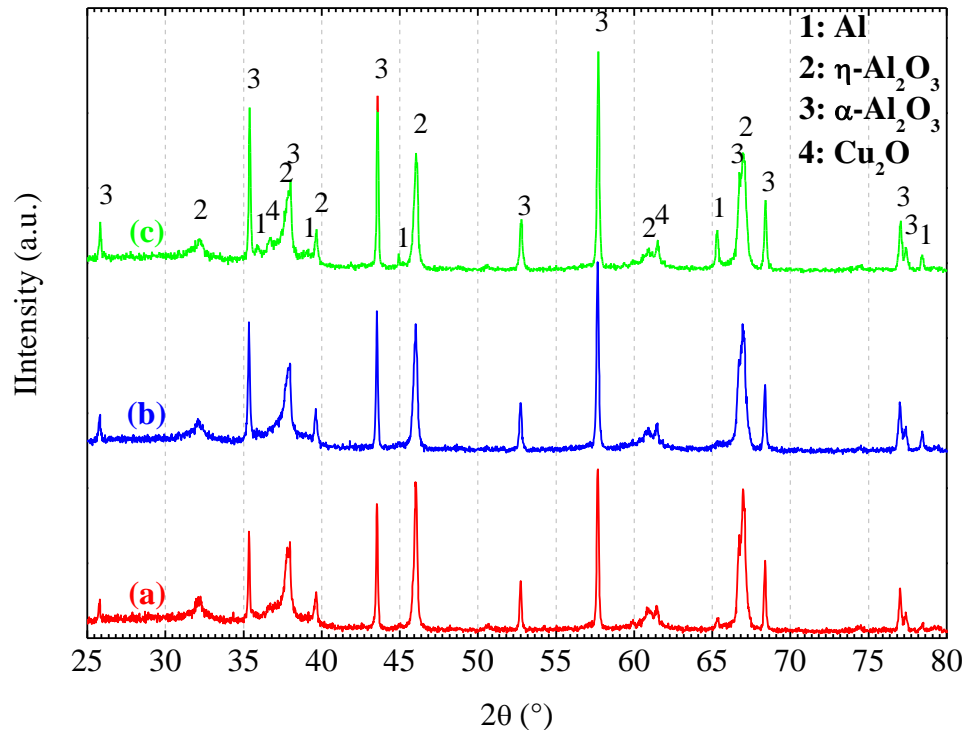


Fig. 16. XRD patterns (using Bragg-Brentano geometry) of the PEO coatings synthesized for 1 hour in various aged electrolytes: (a) 1 h, (b) 4 h and (c) 8 h.

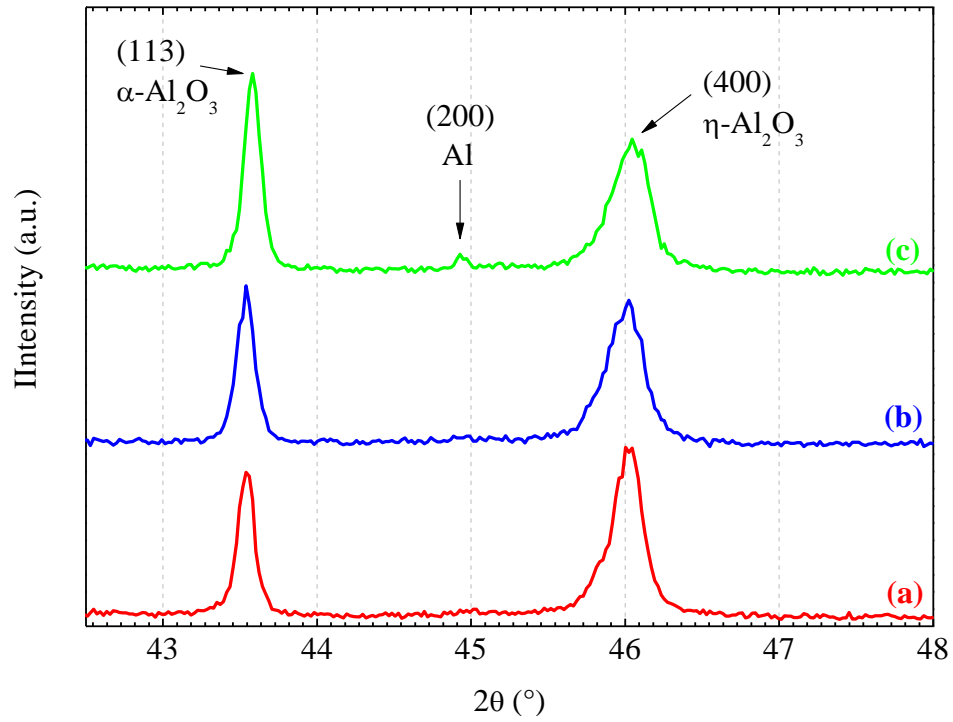


Fig. 17. Selected region of XRD patterns where $(113) \alpha\text{-Al}_2\text{O}_3$ and $(400) \eta\text{-Al}_2\text{O}_3$ peaks are found. Same conditions as in Fig. 16.

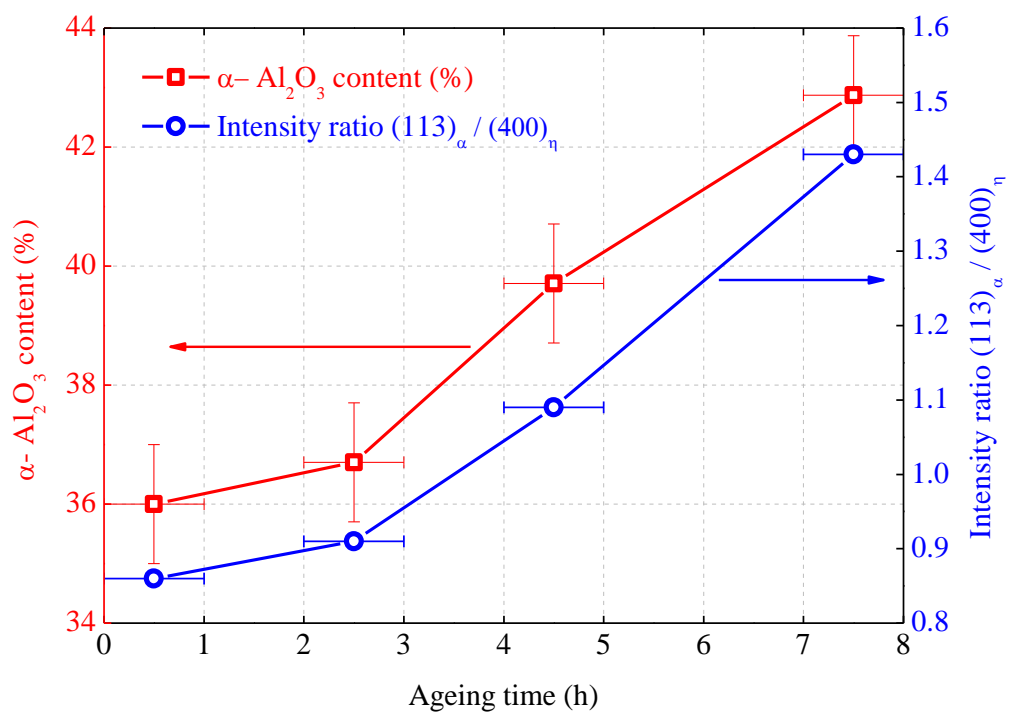


Fig. 18. Variation of the α -Al₂O₃ content in the PEO layers (calculated from XRD measurements carried out at the centre of the processed samples) and variation of the intensity ratio (113) _{α} / (400) _{η} of (113) α -Al₂O₃ and (400) η -Al₂O₃ peaks as a function of the ageing time of the electrolyte.